New Journal of Physics
The open-access journal for physics

Time-averaging within the excited state of the nitrogen-vacancy centre in diamond

L J Rogers[1], R L McMurtrie, M J Sellars and N B Manson
Laser Physics Center, RSPhysSE, Australian National University, Canberra, ACT 0200, Australia
E-mail: lachlan.rogers@anu.edu.au

New Journal of Physics **11** (2009) 063007 (15pp)
Received 20 February 2009
Published 3 June 2009
Online at http://www.njp.org/
doi:10.1088/1367-2630/11/6/063007

Abstract. The emission intensity of diamond samples containing negatively charged nitrogen-vacancy centres are measured as a function of magnetic field along the ⟨111⟩ direction for various temperatures. At low temperatures the responses are sample and stress dependent and can be modelled in terms of the previous understanding of the ^{3}E excited state fine structure which is strain dependent. At room temperature the responses are largely sample and stress independent, and modelling involves invoking a strain independent excited state with a single zero field spin-level splitting of 1.42 GHz. The change in behaviour is attributed to a temperature dependent averaging process over the components of the excited state orbital doublet. It decouples orbit and spin and at high temperature the spin levels become independent of any orbit splitting. One significant implication of this averaging is that it simplifies the development of room temperature applications.

[1] Author to whom any correspondence should be addressed.

Contents

1. Introduction 2
2. Emission variation with magnetic field: room temperature 3
3. Interpretation of room temperature response 3
4. Emission variation with magnetic field: low temperature 6
5. Interpretation of low temperature response 7
6. MCD of zero-phonon line 10
7. Averaging process with temperature 11
8. Conclusion 12
Acknowledgments 13
References 13

1. Introduction

There is interest in using the negatively charged nitrogen-vacancy colour centre in diamond (NV^-) for applications in the area of quantum information processing [1], quantum computing [2]–[5], and magnetometry [6, 7]. The applications rely on the spin in the ground state, and the behaviour of this spin in its environment is largely understood [7]–[11]. The excited state is also used for initialization and for readout, and an understanding of spin in this state has been obtained from low temperature excitation measurements [12]. The state is an orbital doublet which is usually split by internal strain, and the excitation measurements examined the fine structure in both orbital branches. More recently, however, fine structure has also been determined from room temperature optically detected magnetic resonance (ODMR) measurements [5, 13] and it was not clear how these values related to those obtained for the two branches at low temperatures. In this work it is shown that the room temperature results do not correspond to either branch, but rather are due to an averaging of both branches.

The excited state fine structure has been obtained from high resolution optical excitation measurements of single NV centres [12, 14] and from two laser hole burning [15]–[17]. These techniques are applicable at low temperatures but cannot be extended to higher temperatures. On the other hand, spin information has also been obtained from ODMR of single centres [13, 18]. In this case the observations were made at room temperature and the techniques are not readily extended to low temperature. Instead of these techniques, we use level crossing of the spin states as indicated by changes of emission as a function of magnetic field. This approach is applicable over the entire temperature range from room temperature to helium temperatures, and does not require the same level of specialist equipment. Room temperature responses have been reported previously [19], and the close relationship between ensemble and single site results suggested that a study of concentrated crystals could be fruitful. Ensemble measurements using crystals allow uniaxial stress to be introduced; and so the studies can involve variation of the temperature, the magnetic field and the stress. The focus of this investigation was how the averaging process changes the observation between high and low temperatures.

2. Emission variation with magnetic field: room temperature

A sample (designated L) with an NV^- concentration of $10^{-17}\,cm^{-3}$ was aligned with a $\langle 111\rangle$ face parallel to the magnetic field direction. The sample was excited using a 532 nm wavelength laser and the red emission at right angles detected using a Si diode. This emission was monitored as a function of magnetic field and is shown in figure 1(a). There is about a 10% drop in intensity between 0 and 400 G followed by a flatter response, with sharp features at 510 ± 5 and 1028 ± 3 G. The sharp dip at 1028 G occurs when there is an avoided crossing of the ground state spin levels for centres aligned with the magnetic field [19]–[21]. This feature gets narrower with closer alignment of the $\langle 111\rangle$ axis with the magnetic field [22], and adjustment was made to minimize the width. Emission can also be quenched by radio waves. The minimum frequency (20 MHz) at which this could be achieved indicated that the transverse field was about 3 G, and hence the misalignment was less than 0.2°. The emission responses as a function of magnetic field (which we will call 'magnetic spectra') were then measured for angles of 2°, 4° and 6° and these are also shown in figure 1(a). The feature of primary interest is the decrease at 510 G, but it is complicated by cross relaxation with single interstitial nitrogen occurring at the same field value (see section 3).

Uniaxial stress of up to 0.5 GP could be applied using a piston arrangement. It was applied along the $\langle 110\rangle$ direction and transverse to the centres giving rise to 1028 and 510 G features. The results are shown in figure 2 and it can be seen that the stress had almost no effect on the room temperature response.

3. Interpretation of room temperature response

The optical transition associated with the nitrogen-vacancy defect is known to be due to an $^3A_2 \leftrightarrow {}^3E$ transition at a site of trigonal symmetry. Neglecting the orbital doublet nature of the excited state, the dynamics have been described in terms of a 7-level model; three spin levels in the ground state, three in the excited state, and an intermediate singlet level [23]. (The $m_s = \pm 1$ spin levels in the ground and excited states can be degenerate, and if these are treated as single levels the system can be considered as a 5-level system.) These energy levels are shown schematically in figure 3, with transition rate parameters which have been obtained from lifetime measurements and other transient changes in the emission [23]. The dominant terms are those associated with the optical transitions where spin projection is conserved, and those associated with decay via the singlet. The singlet path results in a fraction of the $m_s = \pm 1$ excited spins relaxing to the ground $m_s = 0$ without visible emission, and as a consequence the emission associated with $m_s = \pm 1$ is weaker than that associated with $m_s = 0$. Once the system is cycled several times the population is predominantly in the $m_s = 0$ level (the system is 'spin polarized') and the emission is high. Spin polarization and emission will be reduced whenever the spin states are mixed, and this can occur with the application of an external magnetic field. The mixing introduced by a magnetic field is readily calculated and a rate equation treatment of the 7 levels can be used to predict the changes in the intensity of the emission as a function of the magnetic field (figure 1(b)).

The largest changes occur for magnetic fields giving rise to crossing of the spin levels. For example, the zero field separation between the $m_s = \pm 1$ and 0 spin states in the ground state is 2.88 GHz and so if an axial field of 1028 G ($g = 2$) is applied the $m_s = 0$ and -1 become degenerate. Any additional transverse magnetic field lifts this degeneracy and the basis states

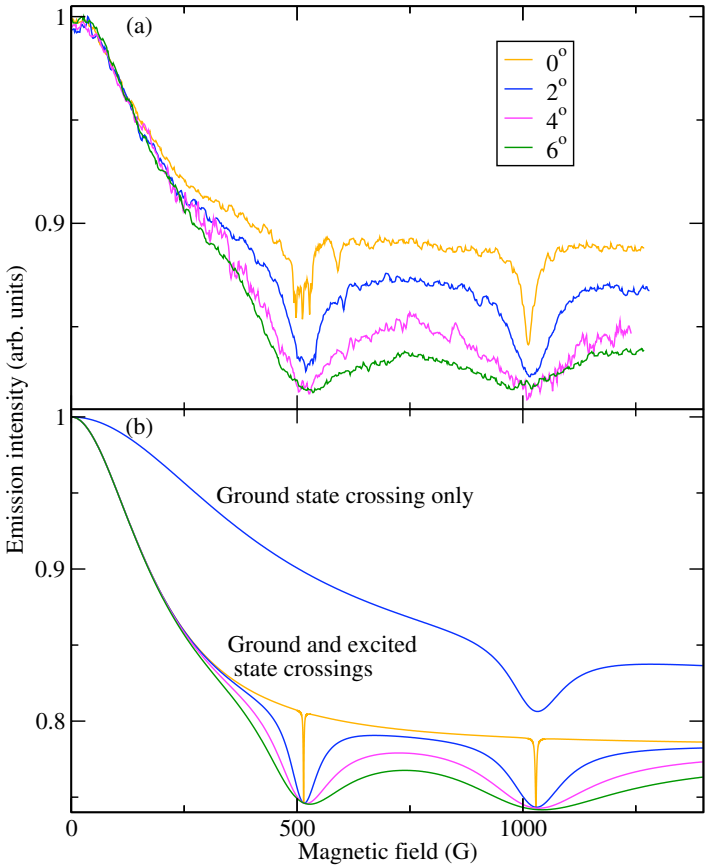

Figure 1. (a) Measured magnetic spectra at room temperature for various misalignment angles as indicated in the common legend. The fine structure on the 510 G feature in the experimental trace for 0° misalignment is due to spin cross-relaxation with nearby nitrogen impurities (see section 3), and is not of interest here. (b) Calculated magnetic spectra for the same misalignment angles, simulating an ensemble sample with four different NV^- orientations. The variation in emission intensity was calculated using rate equations for the 7-level model shown in figure 3. The upper trace shows the effect of spin mixing (spin level avoided-crossing) in the ground state at 1028 G, and the other traces also include similar spin mixing in the excited state at 510 G. The calculation gave a full-depth feature at 510 G for the 0° case, which is incorrect as explained in section 3.

become totally mixed. Spin polarization is no longer maintained and the emission intensity is reduced. This accounts for why there is a sharp reduction in the emission intensity when a magnetic field aligned close to the ⟨111⟩ direction is swept in magnitude through 1028 G. With greater misalignment, and thus a larger transverse field, the spin mixing occurs over a larger range of field and accounts for the broadening of the feature. For ensemble samples the non-axial centres also contribute to the emission and there is an additional change in emission as a function of magnetic field. For a field sweep from 0 to 1400 G the rate equation calculation gives a gradual decrease in emission intensity plus the sharp dip at 1028 G. Such emission changes are observed, but the calculation only allowing for this ground state avoided crossing does not

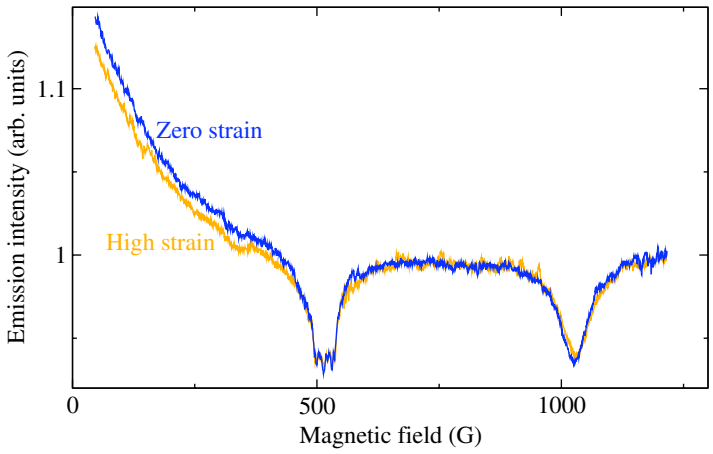

Figure 2. Room temperature magnetic spectra (as in figure 1(a)) with and without 0.35 GP uniaxial strain applied perpendicular to the ⟨111⟩ crystal axis with which the magnetic field was aligned.

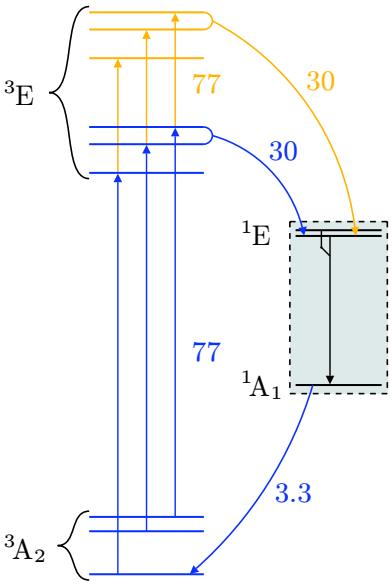

Figure 3. Energy level models used for calculations, with transition rate parameters in units of $10^6\,s^{-1}$ from [23]. Non spin-conserving transitions were included in calculations to give realistic spin polarization levels, but are left off this diagram for clarity. The structure in the intermediate singlets is not important here since the lifetime of the ^{1}E′ level is very short [24], and so the system enclosed in the dashed box can be treated as a single level. The 7-level model includes the three ground spin levels, a single intermediate level and three spin excited state levels (and is shown in blue). To describe the low temperature results, it is necessary to add the three spin levels for the second orbital branch in the excited state (shown in orange) to give a 10-level model.

give good correspondence with the observations as can be seen by comparing the upper trace in figure 1(b) with experimental results in figure 1(a).

In the present work we also consider the effect of a zero field splitting in the excited state. To account for a level crossing at 510 ± 5 G, the zero field splitting is taken to be 1.43 ± 0.01 GHz (with $g = 2$). The effect on the eigenstates can be calculated in the same ways as for the ground state. The excited state avoided crossing causes a decrease at the field value of 510 G which again broadens with misalignment. The contribution of both these crossings in the non-axial centres accounts for initial decrease in emission at low field values. Including both the ground and excited state avoided crossings in the rate equation model was found to give excellent agreement with experiment (figure 1).

However, the rate equation calculation is inaccurate for very small misalignment angles. It assumes that the optical transitions occur between the eigenstates of the ground and excited state, but the excited state lifetime is too short for the system to relax to its eigenstates when the off-axis field is small. The result is that spin polarization and high emission are maintained through 510 G, and the excited state avoided crossing feature disappears for very good alignment. The calculations used above are valid for misalignments greater than 1°, and this is the range considered by the experiments used in this paper.

As just discussed, when the magnetic field is aligned within 1° the axial centres maintain good spin polarization even at 510 G. However, at this field value there is an energy match between the separation of the ground state spins in the NV^- centre and spins in $S = \frac{1}{2}$ centres such as substitutional nitrogens. The spin polarization can be quenched due to a cross relaxation process, and the emission will be reduced. Such a feature can be seen in the 0° misalignment trace on figure 1(a), and it has clear structure. This cross relaxation (including the involvement of changes of nuclear spin projection) has been studied previously [20, 21], [25]–[29], and is not the subject of this paper.

It is concluded that the room temperature magnetic field data can be explained assuming there is an excited state with a single avoided crossing at 510 G. Within experimental uncertainty, this is consistent with an state having a zero field splitting of 1.42 GHz and $g = 2$ as has been observed in the room temperature ODMR measurements [5, 13].

4. Emission variation with magnetic field: low temperature

Magnetic field spectra were recorded for temperatures between 8 and 300 K, and the variation for sample L is shown in figure 4. Due to thermal expansion of the components holding the diamond sample, and thermal variation in absorbtion, it was difficult to keep the absolute magnitude calibrated over a large temperature range. However, the emission is determined by the optical pumping cycle, and at high field will have a fixed value as the spin eigenstates are (to a good approximation) determined by the magnetic field and thus are independent of temperature. The emission responses have, therefore, been normalized to their high field intensities. An exponential fit to the high field tail of the measured spectra allowed each trace to be extrapolated to its asymptotic value.

The 1028 G feature that corresponds to an avoided crossing in the ground state is approximately constant, indicating that the ground state properties do not change with temperature. However, the 510 G feature attributed to the excited state changes dramatically. At room temperature it is centred on 510 G, slightly narrower than the ground state crossing feature, and retains these properties down to 100 K. Cooling further to 40 K causes this feature

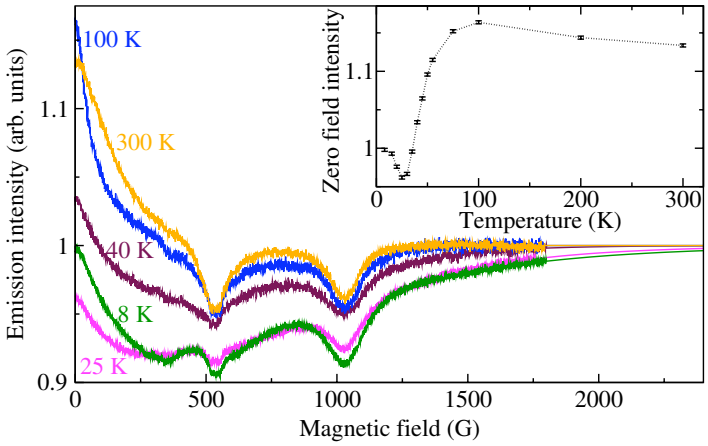

Figure 4. Temperature dependence of the magnetic field spectrum. The spectra have been fitted beyond 1250 G with exponential functions, and normalized at the high field limit. The cross relaxation fine structure at 514 G is not related to the excited state, but provides useful confirmation of the field magnitude. The inset shows the zero field to high field ratio as a function of temperature.

to diminish significantly. By 25 K there is no feature at 510 G (other than the cross relaxation feature), and instead there is a local minimum in the spectrum at about 250 G which is much broader than the ground state crossing. Cooling below 25 K caused a double-bump to appear (figure 4). Also it is noted that as the sample is cooled the emission intensity at zero-field varies significantly (inset in figure 4). It has a minimum at 25 K and a maximum at 100 K. There is a small reduction in zero-field intensity as the temperature increases from 100 K to room temperature.

Unlike the result at room temperature, uniaxial stress was found to alter the magnetic field spectrum at low temperature. Examples are shown in figure 5. Sample L exhibits significant changes with stress. The doublet is changed to single broad feature (plus the cross relaxation feature). The second sample H contained a higher concentration ($10^{18}\,\mathrm{cm}^{-3}$) of NV^- defects and, although barely changed by external stress, already had the characteristics of the first sample with stress applied.

5. Interpretation of low temperature response

At low temperatures fine structure attributed to the ^{3}E state has been observed in hole burning [15]–[17], [30], excitation [12, 14] and photon echo [31, 32] experiments. The Hamiltonian associated with this structure is given by

$$\mathcal{H} = \mathcal{H}_{\mathrm{so}} + \mathcal{H}_{\mathrm{ss}} + \mathcal{H}_{\mathrm{str}} + \mathcal{H}_z, \tag{1}$$

where $\mathcal{H}_{\mathrm{so}}$ is spin–orbit, $\mathcal{H}_{\mathrm{ss}}$ spin–spin, $\mathcal{H}_{\mathrm{str}}$ strain and $\mathcal{H}_z$ the Zeeman interaction. The diagonal component of spin–orbit $\mathcal{H}_{\mathrm{so}} = \lambda_z \mathbf{L}_z \mathbf{S}_z$ splits the state into three equally separated doublets. One doublet (E irreducible representation) is not displaced and associated with the S_z states ($m_s = 0$). The state where spin and orbital projections are parallel (also E irreducible representation) is displaced down in energy by λ_z and the antiparallel alignments (A_1 and A_2 states) are displaced up in energy by the same magnitude. The off-diagonal spin–orbit $\lambda_{x,y}(\mathbf{L}_x\mathbf{S}_x + \mathbf{L}_y\mathbf{S}_y)$ has only

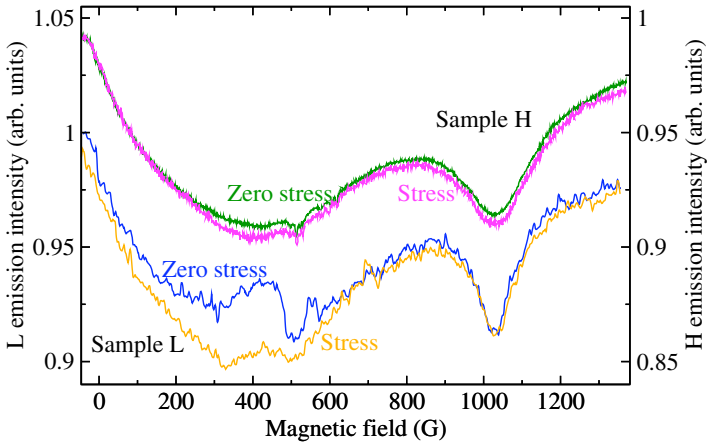

Figure 5. Low temperature (15 K) magnetic spectra with and without 0.35 GP uniaxial stress perpendicular to the ⟨111⟩ crystal axis with which the magnetic field was aligned. The traces for sample H (higher concentration) have been translated up for clarity and correspond to the right-hand vertical axis.

a minor effect as its value is known from previous work to be small ($\lambda_{x,y} = 0.2$ GHz) [12]. Spin–orbit can mix ^{3}E states with singlets, but this has negligible effect on the energy levels. Spin–spin $\mathcal{H}_{ss}$ has two contributions. There is a normal spin–spin term $D_{es}(\mathbf{S}_z^2 - \frac{2}{3})$ which shifts the $m_s = \pm 1$ states with respect to $m_s = 0$ states by D_{es}. The second spin–spin contribution is associated with spins on the two orbital components of the degenerate state [33]. It only affects A_1 and A_2 states and we assign the magnitude of this splitting as Δ. The energy levels in perfect C_{3v} symmetry are therefore shown on the left of figure 6 [12, 34]. The energies are determined by four parameters and the value of the parameters have been obtained from high resolution excitation traces of single centres. The most reliable parameters from recent measurements [14] are $\lambda_z = 5.5$ GHz, $D_{es} = 1.42$ GHz, $\Delta = 3.1$ GHz and $\lambda_{x,y} = 0.2$ GHz.

The splitting of the excited state energy levels with strain, as shown in figure 6(a), can be calculated by diagonalizing the energy matrix

$$\mathcal{H} = \begin{bmatrix} \lambda_z + \frac{1}{3}D_{es} + \Delta & 0 & 0 & 0 & \delta_y & -\delta_x \\ 0 & \lambda_z + \frac{1}{3}D_{es} - \Delta & 0 & 0 & \delta_x & \delta_y \\ 0 & 0 & -\frac{2}{3}D_{es} - \delta_x & \delta_y & i\lambda_{x,y} & 0 \\ 0 & 0 & \delta_y & -\frac{2}{3}D_{es} + \delta_x & 0 & i\lambda_{x,y} \\ \delta_y & \delta_x & -i\lambda_{x,y} & 0 & -\lambda_z + \frac{1}{3}D_{es} & 0 \\ -\delta_x & \delta_y & 0 & -i\lambda_{x,y} & 0 & -\lambda_z + \frac{1}{3}D_{es} \end{bmatrix}$$

where δ_x and δ_y are strain parameters.

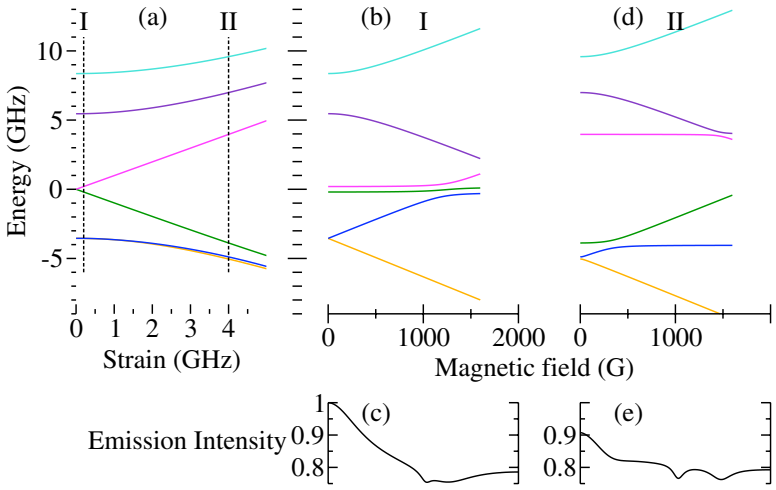

Figure 6. (a) Excited state energy level splittings as a function of strain. (b) Splitting of energy levels for a centre at strain I (0.2 GHz) with a magnetic field applied at 2° to the NV^- axis, and (c) the magnetic spectra calculated for this strain from the 10-level model in figure 3. (d) and (e) show the corresponding responses to an identical magnetic field when the centre is at strain II (4 GHz). The magnetic spectra in (c) and (e) are shown in more detail in figure 7(a), but are included here to indicate their connection with the spin level avoided crossings.

Strain perpendicular to the trigonal axis lowers the symmetry and $\mathcal{H}_{str}$ has the effect of splitting the ^{3}E into two orbital branches each with three spin levels (figure 6(a)) [12, 34]. In the lower branch spin–orbit and spin–spin have opposite signs. At zero strain spin–orbit is larger resulting in the $m_s = \pm 1$ states being lowest. However, spin–orbit splitting is reduced with increasing strain and the separation of the $m_s = \pm 1$ and $m_s = 0$ levels is reduced. The states can cross, although the crossing is changed to an avoided crossing by off-diagonal spin–orbit interaction. The distance of closest approach of these levels enables the strength of the interaction to be determined and a value of $\lambda_{x,y} = 0.2$ has been obtained in this way [12]. In the upper branch, spin–orbit and spin–spin have the same sign and the states are always well separated such that there is little mixing [12, 34].

For low fields (<2500 G) the Zeeman interaction is dominated by $2\mathbf{S}\beta\mathbf{B}$ and the splittings are illustrated in figures 6(b) and (d) for centres with various values of strain. In the case where strain is sufficient to split the ^{3}E state into two triplets (II) each triplet is split analogous to that of an orbital singlet. The important features are the avoided crossings of the $m_s = 0$ and $m_s = -1$ spin levels. There is one associated with each orbital branch. Rate equations for the 10 levels (figure 3) are used to calculate the changes of emission as a function of field. Decrease in emission is obtained at field values corresponding to the two excited state avoided crossings plus the one in the ground. As can be seen from the examples, the magnetic field values at which the excited state dips occur vary with strain and can occur at zero field (figure 7(a)).

For an ensemble the emission will have contribution from centres with a range strain environments, and an example using six strain values is shown in figure 7(b). Reliable calculation would require knowledge of the distribution, but this is not available. However, we can comment on how certain characteristics arise. A contribution from centres with mixing at

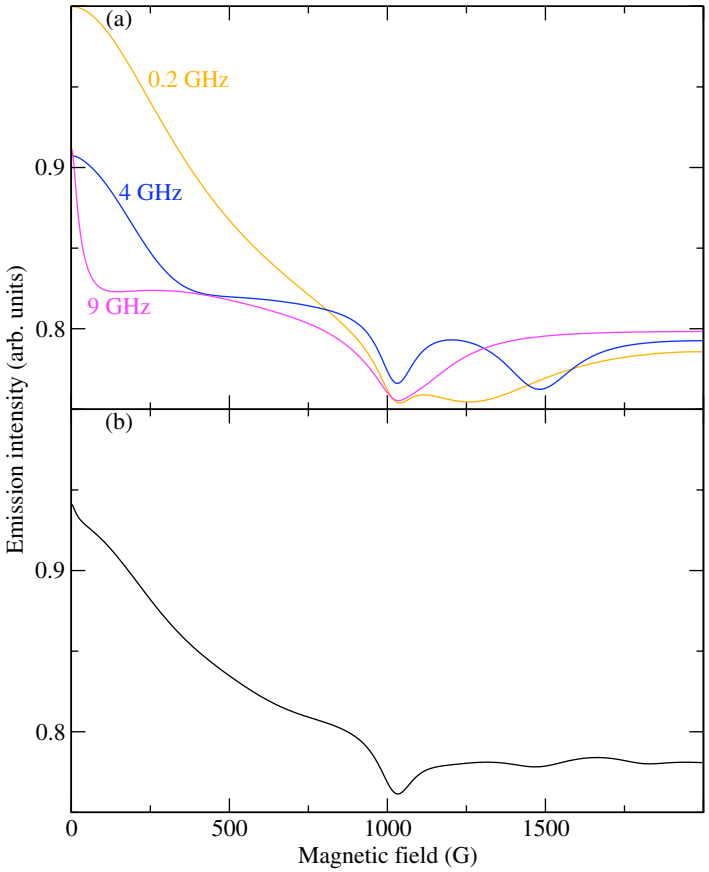

Figure 7. Calculated magnetic spectra, with a field misalignment of 2°, for (a) strain splittings of 0.2, 4 and 9 GHz; and (b) an ensemble with strain distribution. The strain distribution in (b) consisted of 0, 0.2, 2, 4, 7, 9 GHz with corresponding weights of 1, 3, 5, 5, 3, 1. The off-axis NV^- centres are included in these calculations, simulating an ensemble crystal sample.

zero field will depress the emission at zero field and this has been observed in the experiment (figure 4). Also as the avoided crossing in the lower branch always occurs at low field values (<500 G) it is understandable why the emission in the 200–500 G range is low. Conversely avoided crossing in the upper branch occur at higher fields and accounts for the slow increase in emission intensity as the field is extended above 2000 G.

The conclusion is that the low temperature responses are consistent with what is expected from the known fine structure of the NV^- centre and its variation with strain. A variation from centre to centre and sample to sample is understandable in this model, but this is totally different to the behaviour at room temperature.

6. MCD of zero-phonon line

An axial magnetic field splits an orbital E state into two components E_+ and E_- and these components give allowed transitions to an orbital A state in right and left circular polarized light, respectively. Measurements of the electronic transition can be made using modulation

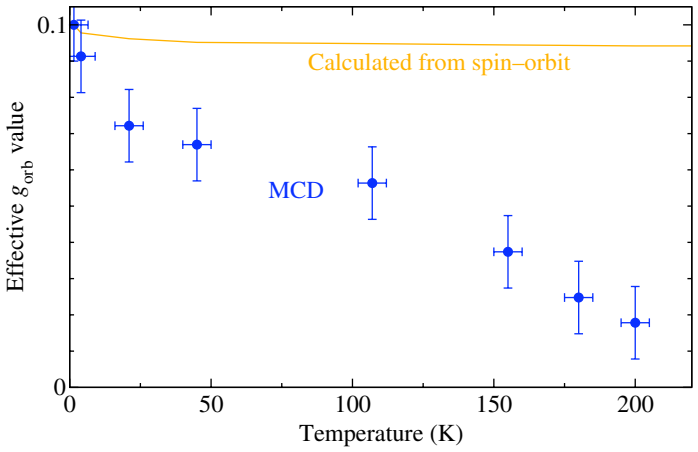

Figure 8. The effective g_{orb} value as a function of temperature, obtained from the first moment of the MCD response, compared with prediction from spin orbit.

techniques, and by using the first moment of the magnetic circular dichroism (MCD) the Zeeman splitting can be determined even in the presence of inhomogeneous broadening [35]. The splitting allows the orbital angular momentum to be determined, which would be temperature independent and for an A $\leftrightarrow$ E transition. The situation here is slightly more complicated as the transition is ^{3}A $\leftrightarrow$ ^{3}E rather than an A $\leftrightarrow$ E. For this case the electronic Zeeman term leads to three sets of A $\leftrightarrow$ E transitions, one for each spin projection ($m_s = 0$, 1 and -1) and the MCD of each has a slightly different magnitude [36]. Spin–orbit interaction has the effect of increasing the MCD for $m_s = -1$ and reducing it for $m_s = +1$. The different magnitudes leads to a temperature dependence of the MCD. However, as spin orbit is only 5.24 GHz the change of magnitude is only 5%, which is much smaller than considered previously [15].

The MCD and absorption of the zero-phonon line at 637 nm were measured for sample H at various temperatures using a field of 5 T. The variation in the first moment normalized to the strength of the absorption gives the effective orbital g-value g_{orb}, and is shown in figure 8. The magnitude of the signal indicates a splitting of 7 GHz consistent with a $g_{orb} = 0.1$ as obtained previously [15]. What is significant, however, is that the signal drops with increasing temperature and is continuing to drop at 200 K. The size of the decrease is much larger the 5% that could be attributed to spin–orbit interaction. The interpretation is that the effective angular momentum is high at low temperature but approaches zero at room temperature. This variation will be discussed below.

7. Averaging process with temperature

The change of behaviour with temperature is attributed to an averaging process. It is well known that increasing temperature gives rise to a variation of the homogeneous line width of optical transitions. Changes of width involve the transitions combining with the absorption and emission of lattice vibrations of slightly different energies. The vibrations also induce transfer between electronic states and give the standard Boltzmann distribution in the population of adjacent states. By considering specific optical line widths we are able to estimate the timescale of such processes. At helium temperatures a $^3A_2 \leftrightarrow {}^3$E line width of 13 MHz has

been observed [37] and is determined by the radiative lifetime of 12 ns. The lifetime does not change with temperature and at higher temperature the larger widths must reflect lifetimes of the coupled electron-vibrational system. For example at intermediate temperatures hole burning gives an estimate of homogeneous line widths and [38] indicate values of the order of 20 GHz at 60 K. Above 180 K the transitions are homogeneously broadened and can be measured by conventional absorption or emission but give rates of 1000 GHz [39].

Vibrations interact with electronic orbit but not with spin. Therefore the fast rates will involve rapid interchange between orbital components of a degenerate state without changing the spin projection. This is what occurs here, and the fast orbital change has significant effect on observations. In large magnetic fields the interchange will be between states E_+ and E_-, with positive and negative angular momentum. Rapid variation will result in an average state with less or no orbital angular momentum. Thus this type of averaging will reduce the effective orbital angular momentum and account for the observed reduction of the MCD.

For strain the interchange will be between orbital component from E_x to E_y with the S_z, S_x, S_y spin projections remaining unaltered. Although the projections stay the same the energies change (see figure 6). Thus normally the ODMR frequency will be a few GHz's different for the two orbital branches. However, rapid change of the orbital branch at a rate of many tens of GHz will alter the situation and the ODMR measurement will give the average frequency rather than two separate frequencies (this is similar to conditions in liquid state NMR). The averaging effectively quenches the contribution of spin–orbit interaction λ_z. Also as S_x spin coupled to E_x and E_y is distributed between the A_1 and A_2 states the averaging quenches the effect of this splitting Δ. The remaining term in the Hamiltonian $D_{es}(\mathbf{S}_z^2 - \frac{2}{3})$ determines the average $S_z \leftrightarrow S_x$ (and $S_z \leftrightarrow S_y$) separation and the ODMR frequency. At high strain the spin–spin would include a strain-dependent term $E_{es}(\mathbf{S}_x^2 - \mathbf{S}_y^2)$, and the ODMR will give two excited state resonances at $D_{es} \pm E_{es}$.

The above averaging process results in an 'average' state with a zero field splitting determined by the spin–spin interaction D_{es} (low strain situation). In order to obtain a fit for recent low temperature high resolution excitation measurements a zero field splitting of 1.42 GHz is required, and this is confirmed from measurements of the separation of the averaged energy of S_z, S_x, S_y levels [14]. Thus there is consistency between the low and high temperature frequencies, and the averaging accounts for the difference between high and low temperature behaviours.

The averaging is not associated with a static Jahn–Teller effect. For modest orbital strain splitting the averaging can result in the appearance of higher symmetry, however, the splitting varies over a large range from zero to thousands of GHz. Clearly, if there is zero strain splitting there is no Jahn–Teller distortion. Also, with very large orbital splittings it is observed that the ODMR signal is split and therefore the system still has low symmetry. In the case of Jahn–Teller the averaging would result in higher symmetry.

8. Conclusion

From this work it is concluded that the spin and optical properties of the NV^- centre are much simpler at room temperature than has previously been anticipated. Thermal vibrations average the orbital components of the excited state and quench all orbital contribution to the relative energy of the spin levels. In effect, the excited state has the properties of an orbital singlet. Spin level energies are determined only by spin–spin interaction, just as they are in the orbital singlet

ground state. This state averaging process is most likely a general phenomenon when thermal transition rates between orbital branches are large compared with the spin–orbit interaction (resulting in an effective decoupling of spin and orbit). This averaging has a prominent effect in the NV^- system due to the very small spin–orbit interaction. At low temperature the thermal transition rates are slowed and spin–orbit interaction does become significant, and so it is necessary to consider both orbital branches of the excited state.

This averaging has implications for many earlier studies of the NV^- centre. For example, it accounts for why previously observed ODMR signals can be explained in terms of a spin triplet associated with a non-degenerate electronic state [13, 18]. It also justifies our use of a 7-level model both here and in previous publications [23] to explain the optical pumping cycle of the NV^- centre at room temperature.

At room temperature there is little variation in optical properties from site to site, which could make it simpler to develop applications. The averaging eliminates the need to seek centres with optimum properties, and justifies determining many properties from ensemble measurements. Counterintuitively, stronger spin polarization is obtained at room temperature than at low temperature, and this is likely to be of considerable interest for the development of quantum devices.

Acknowledgments

We acknowledge fruitful discussions with Vincent Jacques, Fedor Jelezko and Jörg Wractrup (Universitt Stuttgart). We also thank Elmars Kraus (Australian National University) for undertaking the MCD measurements. This work has been supported by Australian Research Council.

References

[1] Wrachtrup J and Jelezko F 2006 Processing quantum information in diamond *J. Phys.: Condens. Matter* **18** S807–24

[2] Jelezko F, Gaebel T, Popa I, Domhan M, Gruber A and Wrachtrup J 2004 Observation of coherent oscillation of a single nuclear spin and realization of a two-qubit conditional quantum gate *Phys. Rev. Lett.* **93** 130501

[3] Jelezko F and Wrachtrup J 2004 Read-out of single spins by optical spectroscopy *J. Phys.: Condens. Matter* **16** R1089–104

[4] Gurudev Dutt M V, Childress L, Togan E, Jiang L, Maze J, Jelezko F, Zibrov A S, Hemmer P R and Lukin M D 2007 Quantum register based on individual electronic and nuclear spin qubits in diamond *Science* **316** 1312–6

[5] Neumann P, Mizuochi N, Rempp F, Hemmer P, Watanabe H, Yamasaki S, Jacques V, Gaebel T, Jelezko F and Wrachtrup J 2008 Multipartite entanglement among single spins in diamond *Science* **320** 1326–9

[6] Balasubramanian G *et al* 2008 Nanoscale imaging magnetometry with diamond spins under ambient conditions *Nature* **455** 648–51

[7] Maze J R *et al* 2008 Nanoscale magnetic sensing with an individual electronic spin in diamond *Nature* **455** 644–7

[8] Takahashi S, Hanson R, van Tol J, Sherwin M S and Awschalom D D 2008 Quenching spin decoherence in diamond through spin bath polarization arXiv:0804.1537

[9] Hanson R and Awschalom D D 2008 Coherent manipulation of single spins in semiconductors *Nature* **453** 1043–9

[10] Jiang L, Gurudev Dutt M V, Togan E, Childress L, Cappellaro P, Taylor J M and Lukin M D 2008 Coherence of an optically illuminated single nuclear spin qubit *Phys. Rev. Lett.* **100** 073001
[11] Felton S, Edmonds A M, Newton M E, Martineau P M, Fisher D, Twitchen D J and Baker J M 2009 Hyperfine interaction in the ground state of the negatively charged nitrogen vacancy center in diamond *Phys. Rev.* B **79** 075203
[12] Tamarat Ph *et al* 2008 Spin-flip and spin-conserving optical transitions of the nitrogen-vacancy centre in diamond *New J. Phys.* **10** 045004
[13] Fuchs G D, Dobrovitski V V, Hanson R, Batra A, Weis C D, Schenkel T and Awschalom D D 2008 Excited-state spectroscopy using single-spin manipulation in diamond *Phys. Rev. Lett.* **101** 117601
[14] Batalov A, Jacques V, Kaiser F, Siyushev P, Neumann P, Rogers L J, McMurtie R L, Manson N B, Jelezko F and Wrachtrup J 2009 Low temperature studies of the excited-structure of nitrogen-vacancy color centers in diamond arXiv:0902.2330
[15] Reddy N R S, Manson N B and Krausz E R 1987 Two-laser spectral hole burning in a colour centre in diamond *J. Lumin.* **38** 46
[16] Manson N B and Wei C 1994 Transient hole burning in N-V centre in diamond *J. Lumin.* **58** 158–60
[17] Santori C *et al* 2006 Coherent population trapping of single spins in diamond under optical excitation *Phys. Rev. Lett.* **97** 247401
[18] Neumann P *et al* 2009 Excited-state spectroscopy of single NV defects in diamond using optically detected magnetic resonance *New J. Phys.* **11** 013017
[19] Epstein R J, Mendoza F M, Kato Y K and Awschalom D D 2005 Anisotropic interactions of a single spin and dark-spin spectroscopy in diamond *Nat. Phys.* **1** 94–8
[20] Holliday K, Manson N B, Glasbeek M and van Oort E 1989 Optical hole-bleaching by level anti-crossing and cross relaxation in the N-V centre in diamond *J. Phys.: Condens. Matter* **1** 7093–102
[21] van Oort E and Glasbeek M 1989 Cross-relaxation dynamics of optically excited N-V centers in diamond *Phys. Rev.* B **40** 6509–17
[22] Martin J P D, Manson N B, Doetschman D C, Sellars M J, Neuhaus R and Wilson E 2000 Spectral hole burning and raman heterodyne signals associated with an avoided crossing in the NV centre in diamond *J. Lumin.* **86** 355–62
[23] Manson N B, Harrison J P and Sellars M J 2006 Nitrogen-vacancy center in diamond: model of the electronic structure and associated dynamics *Phys. Rev.* B **74** 104303
[24] Rogers L J, Armstrong S, Sellars M J and Manson N B 2008 Infrared emission of the NV centre in diamond: Zeeman and uniaxial stress studies *New J. Phys.* **10** 103024
[25] Glasbeek M and van Oort E 1990 Triplet spin coherent transients of fluorescent N-V centers in diamond *J. Lumin.* **45** 426–8
[26] Hanson R, Mendoza F M, Epstein R J and Awschalom D D 2006 Polarization and readout of coupled single spins in diamond *Phys. Rev. Lett.* **97** 087601
[27] Gaebel T *et al* 2006 Room-temperature coherent coupling of single spins in diamond *Nat. Phys.* **2** 408
[28] Hanson R, Gywat O and Awschalom D D 2006 Room-temperature manipulation and decoherence of a single spin in diamond *Phys. Rev.* B **74** 161203
[29] Jacques V, Neumann P, Beck J, Markham M, Twitchen D, Meijer J, Kaiser F, Balasubramanian G, Jelezko F and Wrachtrup J 2009 Dynamic polarization of single nuclear spins by optical pumping of nitrogen-vacancy color centers in diamond at room temperature *Phys. Rev. Lett.* **102** 057403
[30] Redman D, Brown S and Rand S C 1992 Origin of persistent hole burning of N-V centers in diamond *J. Opt. Soc. Am.* B **9** 768–74
[31] Rand S C, Lenef A and Brown S W 1994 Zeeman coherence and quantum beats in ultrafast photon echoes of N-V centers in diamond *J. Lumin.* **60–61** 739–41
[32] Lenef A, Brown S W, Redman D A, Rand S C, Shigley J and Fritsch E 1996 Electronic structure of the N-V center in diamond: experiments *Phys. Rev.* B **53** 13427–40
[33] Lenef A and Rand S C 1996 Electronic structure of the N-V center in diamond: theory *Phys. Rev.* B **53** 13441–55

[34] Manson N B and McMurtrie R L 2007 Issues concerning the nitrogen-vacancy center in diamond *J. Lumin.* **127** 98–103
[35] Shepherd I W 1968 Magnetic circular dichroism of the R_2 band in KCl and KF *Phys. Rev.* **165** 985–93
[36] Davis J A and Fitchen D B 1968 Magnetic circular dichroism of the R′ center in L1F* *Solid State Commun.* **6** 505–7
[37] Tamarat Ph *et al* 2006 Stark shift control of single optical centers in diamond *Phys. Rev. Lett.* **97** 083002
[38] Nisida Y and Mita Y 1990 Hole-burning effect and photochromism of color centers in synthetic diamonds *Diamond Opt. III Proc. SPIE* **1325** 296–303
[39] Davies G 1974 Vibronic spectra in diamond *J. Phys. C: Solid State Phys.* **7** 3797–809